Eur. Phys. J. Plus (2024) 139:946
https://doi.org/10.1140/epjp/s13360-024-05728-5

THE EUROPEAN PHYSICAL JOURNAL PLUS

Regular Article

Determination and analysis of spectral fluorescence cross-sections of bacteria aerosols

Karin Grünewald[1,a], **Thomas Hall**[1], **Lea Fellner**[1], **Arne Walter**[1], **Marian Kraus**[1], **Frank Wilsenack**[2], **Frank Duschek**[1]

[1] Institute of Technical Physics, German Aerospace Center (DLR), Im Langen Grund 1, 74239 Hardthausen, Germany
[2] Bundeswehr Research Institute for Protective Technologies and CBRN Protection (WIS), Humboldtstraße 100, 29633 Munster, Germany

Received: 15 March 2024 / Accepted: 8 October 2024

Abstract Fluorescence cross-sections of single bacteria provide information on the strength of fluorescence response of bacteria for particular excitation conditions and give hints about a possible distinguishability of bacteria by fluorescence techniques. In this report, the fluorescence cross-sections of dry bacteria aerosols are derived from fluorescence spectra by absolute calibration of the measuring system. The fluorescence is measured in a continuous aerosol flow. The aerosol concentration is calculated from microscopic analyses of bacteria samples taken from the aerosol flow. Established calibration methods such as Mie scattering from monodisperse spheres and Raman scattering from water are applied to the same set of fluorescence spectra. The cross-section data obtained are evaluated with regard to their independency from the applied measuring system. The results are compared to data published in the literature. Polarization effects are identified to contribute to the discrepancies between the different datasets.

1 Introduction

Fluorescence cross-sections of single bacteria are key parameters for fluorescence modeling and support the conception of fluorescence-based detection technologies by setting the necessary sensor sensitivities and by providing general information for a classification of agents. The challenging aspect in the derivation of the cross-sections from fluorescence measurements is the precise absolute calibration of the measuring system to eliminate system-specific effects from the fluorescence readings.

While fluorescence cross-section data for most pathogens are not published, datasets on bio-safety level one (BSL-1) are available in the literature [1–7]. The published results range from good agreement between the particular laboratories up to significant deviations. Sivaprakasam et al. [2], for example, found a factor of seven lower cross-sections for single, dry *Bacillus subtilis* vegetative cells compared to the cross-sections reported by Seaver et al. [1] for *Bacillus subtilis* cells in liquid suspension. Faris et al. [5] noted a factor of four larger cross-sections for the wet suspensions compared to the dry aerosols. In the same paper, an error factor of two is attributed only to uncertainties in the determination of bacteria numbers. Seaver et al. [1] found discrepancies up to a factor of seven for measurements of *Bacillus subtilis* in comparison with results from Sandia National Laboratory and attributed the differences to different bacteria strains and growth media. The authors also refer to the *Brucella* ERDEC (Edgewood Research, Development, and Engineering Center) internal report, where a factor of 25 difference was found for two strains of *Brucella abortus* grown to the same stage with the same media. Further reasons for deviating results are summarized and discussed by Pan et al. [3, 4]. Different preparation methods, storage times, aerosolization conditions, and bacteria sizes are identified to influence the derived cross-section data as well as a possible impact by the illumination intensity. Inaccuracies also occur by contamination due to particles from previous runs that stick in the measuring volume. Calibration uncertainties raise from uncertain sphere sizes and poorly specified complex refractive indices, possible residue surfactants, different spatial distributions of calibration spheres, and sample bacteria as well as from different angular distributions of scattering and fluorescence.

In this work, fluorescence cross-sections of dry bacteria aerosols are derived from fluorescence spectra by absolute calibration of the measuring system using two different optical methods (Raman and Mie scattering). The elaboration of the results will add unintentionally occurring polarization effects in calibration and measurement as a further potential cause to the list of arguments. Moreover, information on the distinguishability of bacteria vegetative cells and spores is derived from the correlation of fluorescence cross-section spectra and discussed for *Bacillus subtilis*, *Escherichia coli*, and *Micrococcus luteus*.

[a] e-mail: Karin.Gruenewald@dlr.de (corresponding author)

Published online: 28 October 2024

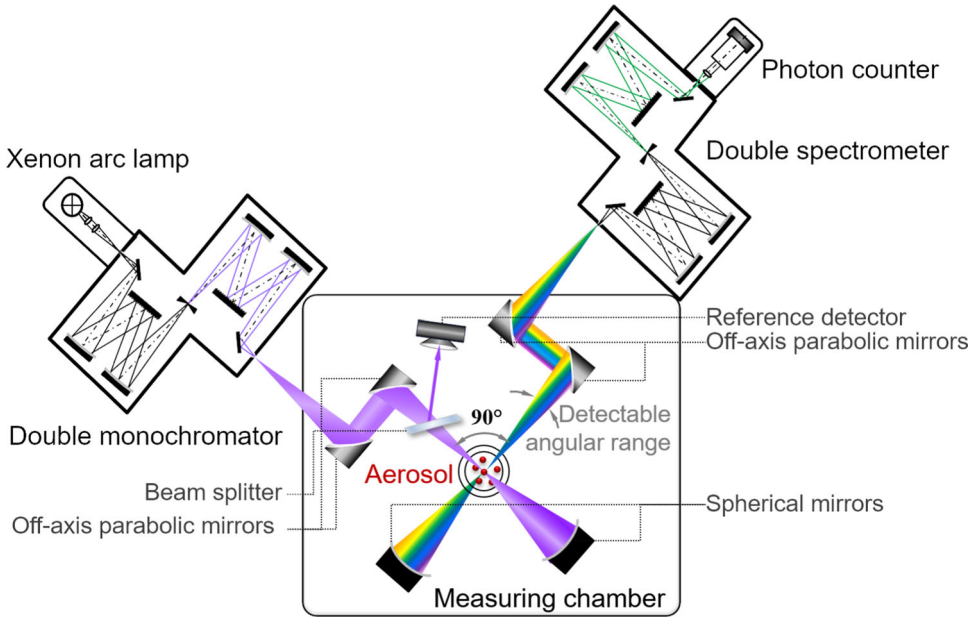

Fig. 1 Top view on optical setup; excitation path and measuring path at an angle of 90°

2 Experiment

2.1 Optical setup

A xenon-arc lamp (HORIBA Scientific FL-1039, USHIO UXL 450SO) is used for excitation. The excitation wavelength is selected by means of a double monochromator (HORIBA Scientific Gemini 180). The position of the monochromator gratings is adjusted to the xenon emission peak at 467.3 nm. The lamp performance is monitored by reference measurement behind the monochromator. Fluorescence and scattering are detected by a Peltier-cooled photon counter (PR Products for Research Inc., Hamamatsu Photonics R4220P select). The detectable angular range is oriented at 90° toward the excitation path. A second double monochromator (HORIBA Scientific Gemini 180) is used to realize the spectral resolution of the fluorescence readings. The position of the spectrometer gratings is adjusted to the wavelength of the Ovalene fluorescence peak (Starna Scientific Ltd. 6BF Series Polymer Block References, Block 2) at 482 nm. Two spherical reflectors enhance the radiation in the measuring volume. The size of the measuring volume is defined by the slit dimensions of the two spectrometers. The measuring section is housed in a measuring chamber. The optical setup is illustrated in Fig. 1.

2.2 Aerosol generation and control

As an alternative to single-particle systems, the present bio-aerosol system provides a continuous aerosol flow of particle concentrations in the range of 10^8 particles/m^3 to several 10^{10} particles/m^3. The fluorescence is measured in the steady flow that is generated from a watery dilution. Aerosol generation and control, as illustrated in Fig. 2, is operated via a programmable logic controller (PLC SIMATIC S7-300) to ensure the reproducibility of the test conditions and to enable BSL-2. A commercial aerosol generator (Palas GmbH AGF10) driven by nitrogen is used to aerosolize the bacteria from the watery dilution. About 90% of the produced aerosol particles are in a size range up to 1 μm in diameter. The wet aerosol is carefully dried in a heat exchanger and fed to a measuring section that is sheathed only by nitrogen flow. Behind the measuring section, the aerosol can pass an aerosol spectrometer (Grimm Aerosol Technik Portable Aerosol Spectrometer PAS 1.109) before it is sucked into filters. Alternating to the fluorescence acquisition phases, the aerosol is fed onto sample filters for predetermined time periods.

The sample filter sheets can be removed from the system for offline microscopical analyses. A laser scanning microscope (Olympus LEXT OLS4000) and a SEM (scanning electron microscope JEOL JSM-IT200) give information on the physical conditions of the bacteria extracted from the aerosol flow. Microscopic images are taken from 13 to 33 different positions on the sample filter to monitor the homogeneity of occupancy distribution and to calculate the bacteria density in the aerosol. A mapping of the analyzed filter positions and a SEM image of *Micrococcus luteus* vegetative cells are shown in Fig. 3. The microscopical bacteria counting can be assisted by the readings of the aerosol spectrometer. Life-dead analyses are performed on a random basis to assess the aerosolization stress on the bacteria. The bacterial viability is tested by using LIVE/DEAD™ BacLight™ Bacterial Viability Kit (Invitrogen, Carlsbad, US) according to the manufacturer. Here, the integrity of bacterial membrans is investigated by two different fluorescence dyes and visualized by ZEISS Axio Imager 2 with Colibri Multicolor LED Light Source. The occupancies of sample filters and the residual dilutions are examined after the fluorescence tests are completed. The results of the life/dead analyses differ

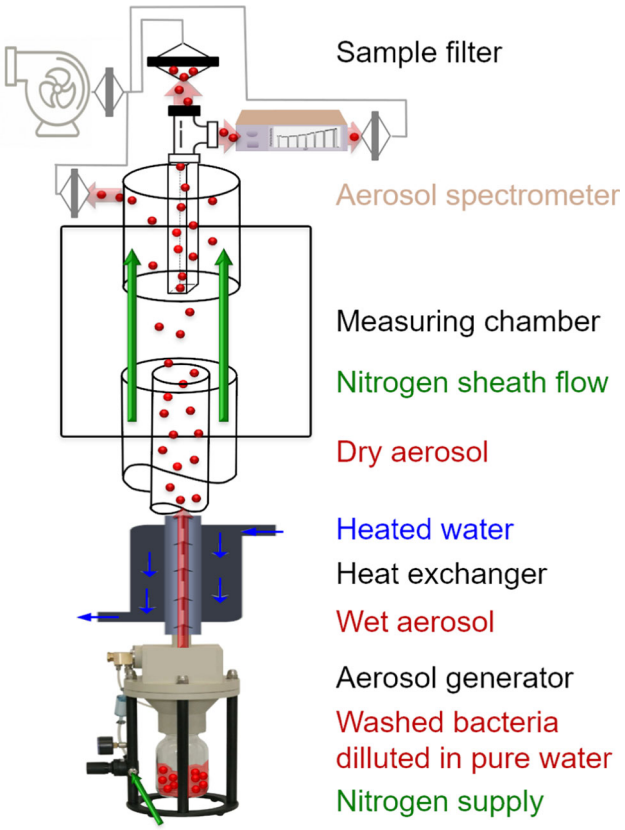

Fig. 2 Aerosol provision

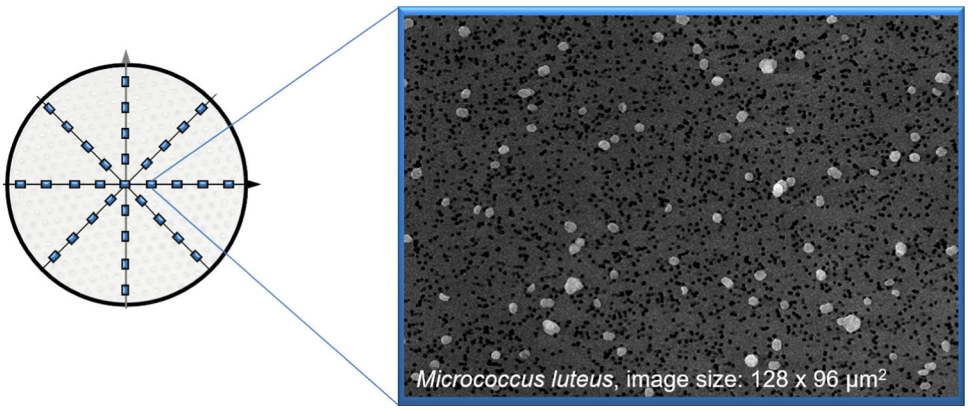

Fig. 3 Bacteria monitoring and counting by microscopic analyses of sample filter occupancies

slightly between the three bacteria species. Still, most vegetative cells survive the aerosolization and measurement phases, as depicted in Fig. 4, again using the example of *Micrococcus luteus*.

2.3 Sample preparation

For the preparation of vegetative cells, bacteria are grown on nutrient agar (Sifin, Berlin, Germany) overnight at 37 °C. At test day, the bacteria are harvested, suspended in ultrapure water (Sartorius Arium® Mini Ultrapure Water System), and centrifuged at 3500 x *g*. The pellets are suspended in ultrapure water to concentrations between 10^9 cfu/ml and 10^{14} cfu/ml. For the preparation of spores, *Bacillus subtilis* is grown on a medium containing 8 g/l nutrient broth, 20 g/l agar, $7.2 \cdot 10^{-4}$ M $CaCl_2$, $3 \cdot 10^{-4}$ M $MnSO_4 \cdot H_2O$, $2 \cdot 10^{-5}$ M $ZnSO_4 \cdot 7H_2O$, and $2 \cdot 10^{-5}$ M $CuSO_4 \cdot 5H_2O$ at 37 °C until sporulation for approximately 15 days. Spores are purified by iterative washing with ultrapure water and centrifuged at 4000 x *g* for 20 min between washing steps. Purity of spores is checked by phase microscopy. Spores are stored at 4 °C until measurement. The final bacteria suspension, vegetative cells or spores, is applied immediately after preparation. The bacteria examined in this report are *Escherichia coli* (DSM18039), *Micrococcus luteus* (DSM20030), and *Bacillus subtilis* (DSM1970) from the German Collection of Microorganisms and Cell Cultures GmbH (DSMZ). Samples of ultrapure water are prepared for background measurements.

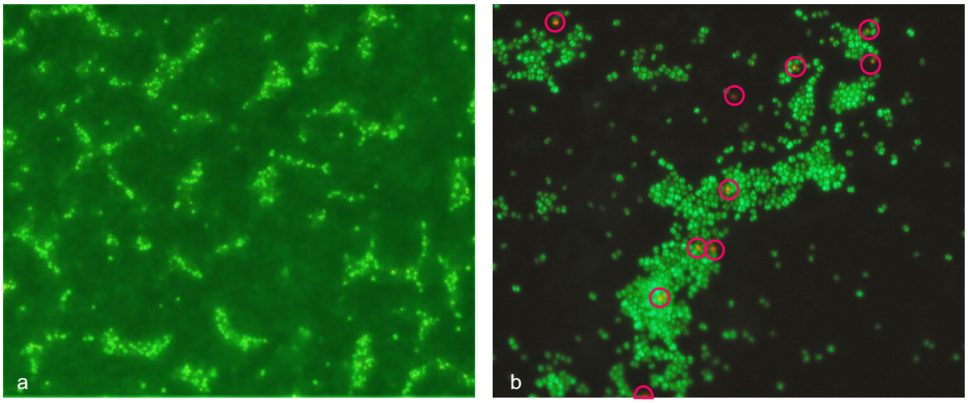

Fig. 4 Results of life/dead analysis using the example of *Micrococcus luteus* vegetative cells (green = alive/red = dead). A sample filter occupancy is pictured on the left (a), and the residual suspension after the fluorescence tests is pictured on the right (b). The positions of red spots ("dead" bacteria) are highlighted by red circles

Chemical samples are provided for calibration purposes. The well-described laser dye DCM [8] is used for emission measurement. DCM (Merck KGaA Sigma-Aldrich 10^{-5} g/ml) is diluted in ethanol (Merck UVASOL® 99.9 %) to concentrations of about $5 \cdot 10^{-7}$ to $1 \cdot 10^{-6}$ mol/l and filled into 3.5 ml Suprasil® cuvettes (Hellma® Article No. 111-10-40, cell path length 10 mm). The concentration is verified by absorption measurement with an extinction factor of $4.25 \cdot 10^4$ L mol^{-1} cm^{-1} at a wavelength of 472 nm. Ethanol samples are prepared for background measurement. Monodisperse spheres (microParticles GmbH NIST-traceable polystyrene particle size standards) delivered as 2 wt% solution with the stabilizer lauryl sulfate at 0.07 wt% and the preservative NaN_3 at 0.007 wt% are diluted in ultrapure water for particle densities up to $7.5 \cdot 10^{12}$ m^{-3}. Dilutions are prepared for Mie scattering measurement with spheres of 497 nm, 320 nm, and 197 nm in diameter. The dilutions contain residual fractions of lauryl sulfate and NaN_3. Sample dilutions of the according concentrations are prepared for background measurement. A purity water sensitivity reference (Starna Scientific Ltd. RM-H2O) is applied for Raman measurement and an empty cuvette for the corresponding background control.

3 Calibration

The derivation of bacterial fluorescence cross-sections necessitates the absolute calibration of the measuring system, excitation path and emission measuring path, to achieve the power of the aerosol excitation and to obtain the power of the fluorescence emission, both as absolute values in physical units. The fluorescence emission is assumed to be isotropic in this approach.

3.1 Calibration methods

The intensity of the fluorescence excitation is derived from calibration measurements that yield the spectral power of the incident light at the position of the aerosol. For this purpose, DCM is applied as calibration substance by placing a cuvette with the characterized test solution in the measuring section. The spectral excitation power is achieved by relating the readings of the DCM emission excited by the xenon-arc lamp to that excited by a laser reference.

In the emission measuring path of the system, the fluorescence photon counts depend on the quantum efficiency of the detector, the efficiencies of the spectrometer gratings, and on the properties of the optical components between aerosol and detector. All these influences have to be eliminated by absolute calibration to extract the power of bacteria fluorescence from the plain, background-adjusted fluorescence readings. Two established methods for absolute calibration are Mie scattering from monodisperse spheres [2, 3] and Raman scattering from water or nitrogen [1, 5]. Each spectral calibration function is achieved by relating the measured data to the corresponding theoretical values of the respective scattering process, considering identical sample conditions and geometries in theory and experiment. For Mie scattering measurement, a cuvette with the watery dilution of monodisperse spheres is placed in the measuring section. The numerical calculations of the scattering functions follow the code published by Wiscombe [9, 10]. The cross-sections for Mie scattering from ideal single spheres [11] are derived according to the referenced approaches [12, 13]. The applied refractive indices of polystyrene [14], air [15], water [16], and Suprasil® [17] cover the sprectral range of interest. The Mie scattering power is calculated from the derived scattering cross-sections, the excitation power, and the particle density in the measuring volume. For Raman scattering measurement, the high-purity water reference is placed in the measuring section. The measured Raman peaks are integrated to gain the experimental data of Raman scattering. The theoretical power values are derived from published Raman scattering cross-sections [18], the excitation intensity, and the molecule density in the measuring volume.

All calibration results are background-adjusted by repeating the above measurements with the respective background samples and extracting the readings from the actual measurements before evaluation.

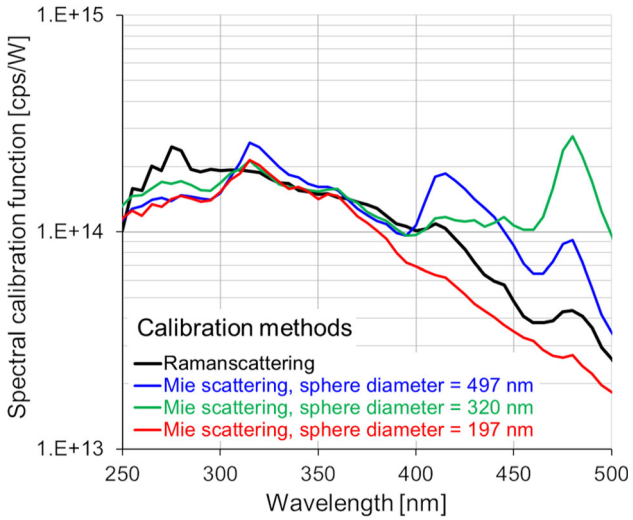

Fig. 5 Spectral calibration functions for identical system conditions derived by Raman scattering from pure water and Mie scattering from monodisperse spheres of different sizes

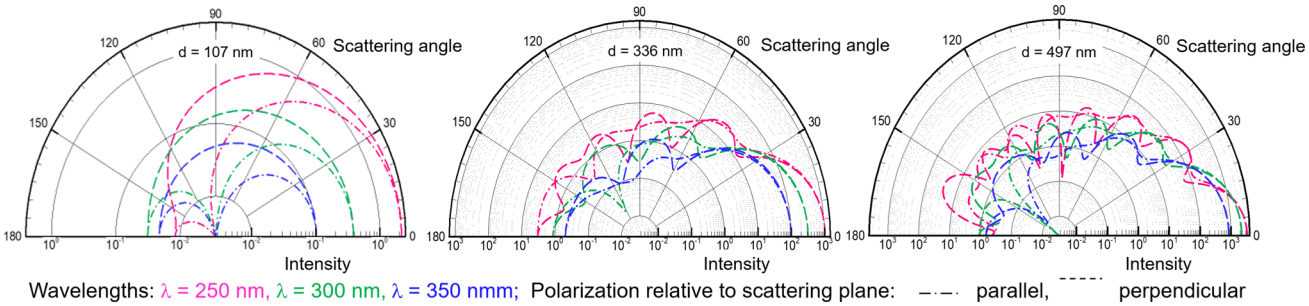

Fig. 6 Mie scattering functions by their polarization fractions in the half-planes of ideal spheres of different diameters d at different wavelengths λ

3.2 Impact of calibration methods

Both calibration methods for the emission measuring path should yield the same spectral calibration functions. As shown in Fig. 5, merely satisfying accordance is achieved for wavelengths below 360 nm. The sectionally averaged root-mean-square amounts to 14 % between 250 nm and 300 nm and 6 % between 300 nm and 360 nm. Above 360 nm, the calibration curves show increasing deviations in value and shape with increasing wavelengths. The root-mean-square reaches a maximum of 90 % at 475 nm. Strong correlation with a correlation factor of 0.91 is achieved between the calibration curves of Raman scattering from water and Mie scattering from spheres of 197 nm in diameter. The strongest differences between the calibration functions occur within the Mie scattering method, solely by using different sphere sizes for calibration. This behavior can be attributed to the strong polarization effects of Mie scattering, depending on sphere sizes, wavelengths, and scattering angles. The polarization effects are illustrated in Fig. 6 using the example of three sphere sizes and unpolarized excitation. The parallel and perpendicularly polarized fractions of the calculated scattering functions are plotted in the scattering half-planes for three excitation wavelengths, each. The angle-dependent variations in polarization increase with increasing sphere diameter for fixed wavelengths, i.e., with increasing Mie size parameter $\chi = \pi d/\lambda$ that relates the sphere diameter d to the wavelength λ.

Figure 7a shows the corresponding degrees of polarization, defined as $\rho = (I_{||} - I_{\perp})/(I_{||} + I_{\perp})$ with the parallel and perpendicularly polarized fractions $I_{||}$ and $I_{\perp}$, respectively. The polarization degrees significantly vary by amount and shape even within the small angular range accessible to the detector around the measuring direction of 90°. The reference data for the grating efficiencies of the spectrometer are depicted in Fig. 7b. The polarization-sensitive gratings process the scattered radiation so that the same amount of intensity may yield to different results at the subsequent detector, depending on the respective polarization of the emitted radiation. The theoretical values are unaffected by such distortions. As a consequence, the spectral calibration functions of Mie scattering result in different curves for different sphere sizes.

Polarization analyses of the Raman scattering readings are performed by measuring the parallel and perpendicularly polarized fractions at the photon counter. The analyzer is positioned in the emission measuring path directly behind the measuring section. The readings are integral over the accessible angular range. The results yield the known frequency-dependent polarization of Raman scattering spectra [19]. When the same analyis is applied to the fluorescence measurement of bacteria vegetative cells diluted in pure water, a varying polarization is measured along the fluorescence spectra. Figure 8 shows the spectral polarization degrees of the fluorescence readings for spherical- and rod-shaped bacteria at an excitation wavelength of 280 nm. The two spectra show no

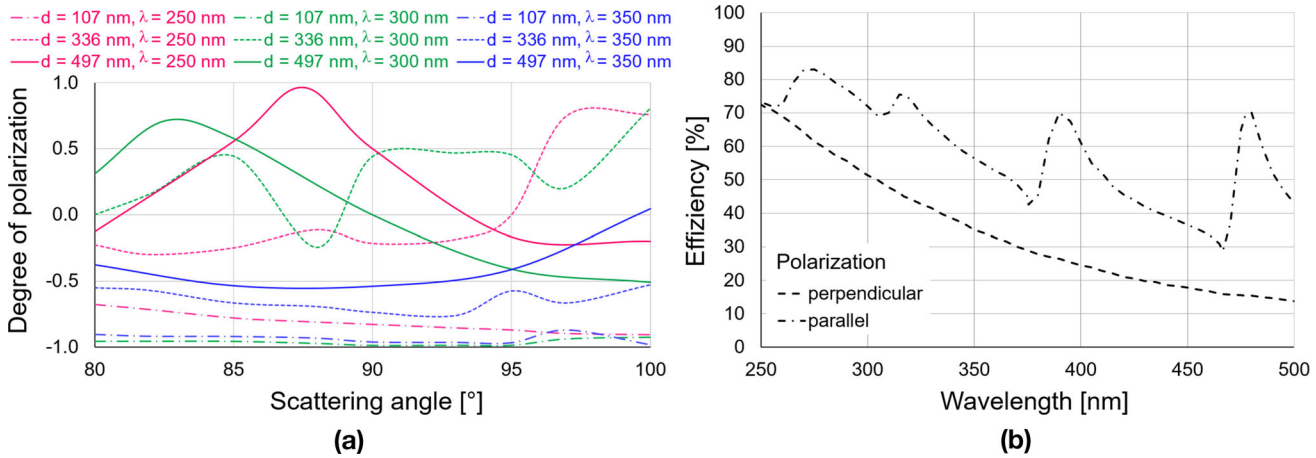

Fig. 7 The polarization degrees of the presented Mie scattering functions within the angular range accessible by the detector (**a**). Reference data for the polarization-dependent efficiencies of the spectrometer gratings (**b**). The polarization directions are related to the scattering plane

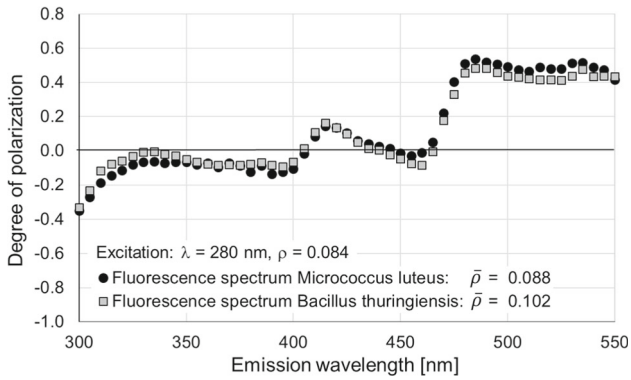

Fig. 8 Spectral polarization degrees of bacteria fluorescence readings together with their particular total values $\overline{\rho}$ integrated over the spectral range

significant differences. With an approximate weight of 10^{-12} g, bacteria exceed the upper limit of about 15 kDa for depolarization by rigid bodies (particle rotation time higher than fluorescence decay time) [20]. These conditons indicate that the polarization results can be attributed to the behavior of the bacterial fluorophores [21]. The three optical processes, Mie scattering, Raman scattering, and fluorescence show different polarization behaviors with the most complex for Mie scattering. As a consequence, the calibration methods lead to deviations of the cross-section spectra even if applied to the same set of fluorescence readings. The results are illustrated in Fig. 9 using the example of *Micrococcus luteus* for an excitation wavelength of 280 nm. The derived cross-section data vary up to one order of magnitude for emission wavelengths above 460 nm. The polarization impact of the present measuring system is evident due to the strong polarization dependence of the grating efficiencies. But polarization effects occur in any optical measuring system, by polarizing properties and/or polarization sensitivities of optical components and detectors [22, 23]. Therefore, the polarization characteristics of calibration and measuring processes should show at least similar behaviors to reduce inherent inaccuracies. In the cross check of Fig. 10, the deviations of the polarization degrees of the applied calibration methods from the polarization degrees of bacteria fluorescence readings are illustrated at three emission wavelenghts for Mie scattering and six emission wavelengths for Raman scattering. Spherical- and rod-shaped bacteria are taken into account. Raman scattering proves to be the better match in the comparison and is the preferred calibration method for the present system. A further advantage of Raman scattering is the continuous availability of pure water standards in contrast with the uncertain availability of spheres of a specific size. A further improvement toward accuracy could be achieved by using the same optical process for calibration and measurement, for example, by applying fluorescing spheres with quantitatively specified excitation-emission maps [24] when available on the market for UV excitation. Those spheres will act as rigid bodies. However, in combination with a calibration by Raman scattering, an additional calibration by fluorescing spheres can limit the area of calibration uncertainty.

4 Fluorescence cross-sections of single bacteria

The following diagrams illustrate the spectral fluorescence cross-sections of single bacteria derived by Raman calibration. Figure 11a shows a comparison of vegetative cells of *Bacillus subtilis*, *Micrococcus luteus*, and *Escherichia coli* for an excitation wavelength of 266 nm. The strength of the overall fluorescence response is achieved by integrating the particular cross-section spectra resulting

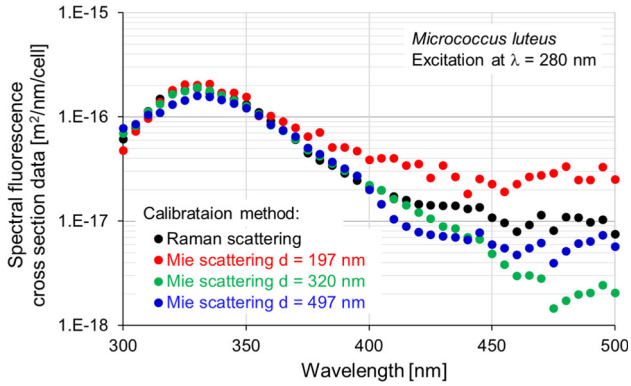

Fig. 9 Fluorescence cross-section data resulting from identical fluorescence readings within the identical measuring system but by application of different calibration methods

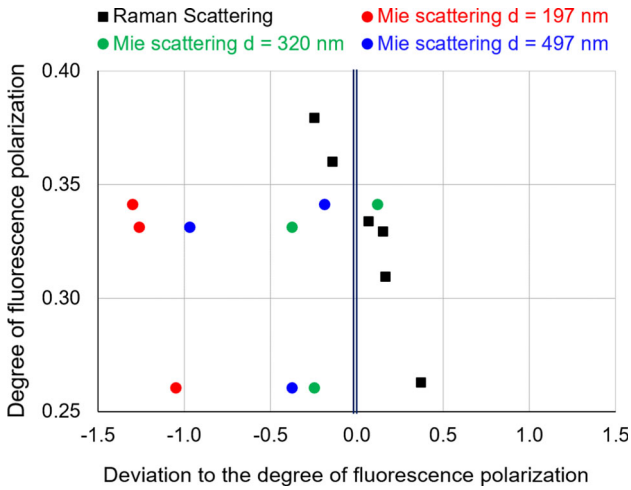

Fig. 10 Deviation of polarization degrees of the calibration methods from the polarization degrees of bacteria fluorescence for randomly selected emission wavelengths

Table 1 Total fluorescence cross-sections for different excitation wavelengths

Wavelengths	266 nm	280 nm	355 nm
B. subtilis vegetative	$1.7 \cdot 10^{-16}$ m^2/cell	$2.6 \cdot 10^{-16}$ m^2/cell	$9.8 \cdot 10^{-18}$ m^2/cell
B. subtilis spores	$2.7 \cdot 10^{-16}$ m^2/spore	$5.2 \cdot 10^{-17}$ m^2/spore	$6.7 \cdot 10^{-18}$ m^2/spore
E. coli	$7.6 \cdot 10^{-17}$ m^2/cell	$9.4 \cdot 10^{-17}$ m^2/cell	
M. luteus	$3.2 \cdot 10^{-17}$ m^2/cell	$5.7 \cdot 10^{-17}$ m^2/cell	$2.5 \cdot 10^{-18}$ m^2/cell

in the total fluorescence cross-sections. The total values for the spectra in Fig. 11a are distributed over approximately one order of magnitude, as to be seen in Table 1.

An illustration of a possible distinguishability of bacteria by fluorescence techniques is achieved by normalizing the spectra at the same emission wavelength, as shown in Fig. 11b. Each spectrum is related to its specific cross-section value at an emission wavelength of 335 nm. The wavelength is chosen close to the particular maximum. The bacteria species show almost identical spectra up to a wavelength of 400 nm with only slight differences above. A comparison of the fluorescence cross-sections of *Bacillus subtilis* vegetative cells and spores follows in Fig. 12a for the excitation wavelengths of 266 nm, 280 nm, and 355 nm. The normalized diagrams on the right of Fig. 12 give a descriptive internal comparison for selected cross-section spectra. The spectra of vegetative cells and spores show satisfying distinguishability at an excitation wavelength of 280 nm, as presented in Fig. 12b. The two cross-section spectra of vegetative cells in Fig. 12c show no pronounced differences. The close excitation wavelengths of 266 nm and 280 nm do not selectively address the different fluorophores of the bacterium. Total values of fluorescence cross-sections are summarized in table 1. The correlation matrix in Fig. 13 gives an overview of a possible bacteria distinguishability by the correlation coefficients of the fluorescence cross-section spectra of vegetative cells and spores for excitation wavelengths of 266 nm and 280 nm. All vegetative cells show correlation coefficients above 0.9 with only weak but recognizable graduation. Significant differences are only found between the spectra of vegetative cells and the spores' spectra excited at 280 nm. Since the correlation between the fluorescence cross-section spectra of the investigated species has emerged as being very strong, efforts toward an appropriately reliable, fluorescence-based differentiation of bacteria should consider all available information. This includes optimized multi-wavelength excitation, fluorescence decay time [25], and, eventually, fluorescence polarization. However, the task will challenge the tools of artificial intelligence. A review of methods and optical techniques for bio-agent detection is given in [26].

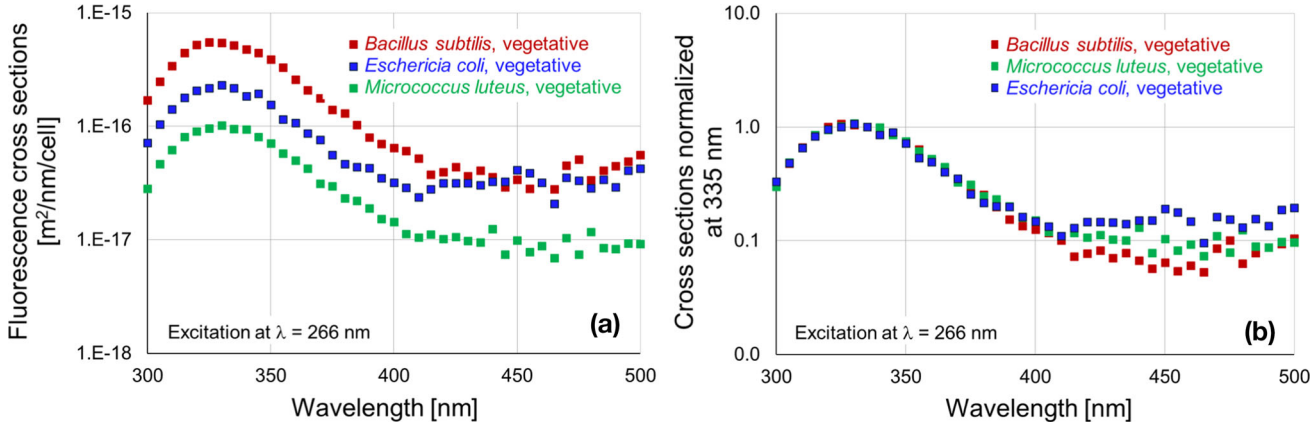

Fig. 11 Comparison of spectral fluorescence cross-sections of different bacteria species at the identical excitation wavelength, absolute values in diagram (**a**) normalized values in diagram (**b**)

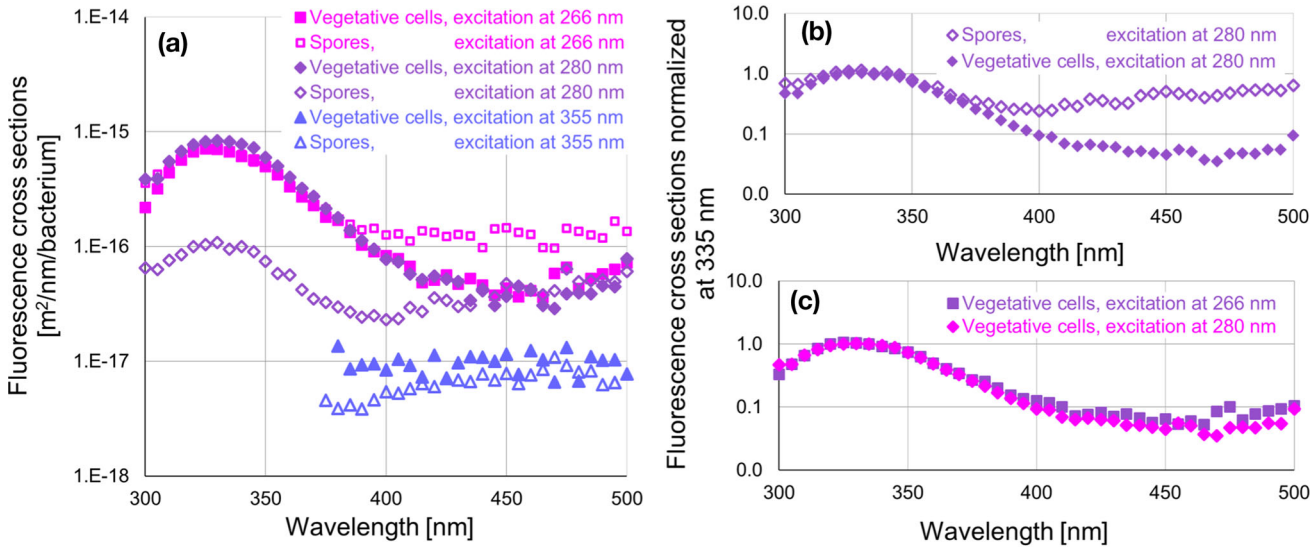

Fig. 12 Intra-comparison of spectral fluorescence cross-sections of *Bacillus subtilis* vegetative cells and spores at different excitation wavelengths with absolute values in diagram (**a**). Exemplary comparison between cells and spores at identical excitation wavelength in diagram (**b**) and exemplary comparison between cells at different excitation wavelengths in diagram (**c**), both comparisons represented by normalized values

While fluorescence cross-section data of most pathogens are not open, the literature provides a broad dataset of cross-sections for bacteria on BSL-1. Due to the specific tasks and conditions of the individual laboratories, direct one-to-one comparisons of the datasets are not possible. Reasonably comparable conditions are gained by adapting the referred data [2, 3] (reviewing also [5–7, 27, 28]) [4] concerning spectral resolution and by compromises toward aerosol conditions and excitation wavelengths. Figure 13 shows a comparison between the presented cross-sections and literature data. Significant deviations, mainly found at emission wavelengths around 450 nm, can largely be attributed to the calibration by Raman scattering instead of by the Mie scattering method that is widespread in the community (Fig. 14). Unspecifiable polarization influences in the particular measuring systems also contribute to the deviations, besides the reasons mentioned in [3, 4].

5 Conclusion

Polarization effects have to be considered for improved reliability of the derived fluorescence cross-sections. Both conventional methods of absolute calibration, Mie scattering and Raman scattering, are affected by polarization impact. Deviations up to one order of magnitude can follow from calibrations by Mie scattering only by a variation of the applied sphere sizes. In the present system, Raman scattering is found to be the preferable calibration method to diminish polarization-dependent inaccuracies. Less polarizing or less polarization-sensitive components will improve the effort as well as a calibration method that is based on the same optical process as the measurement, i.e., for example, by using certified fluorescing microspheres with quantitatively specified

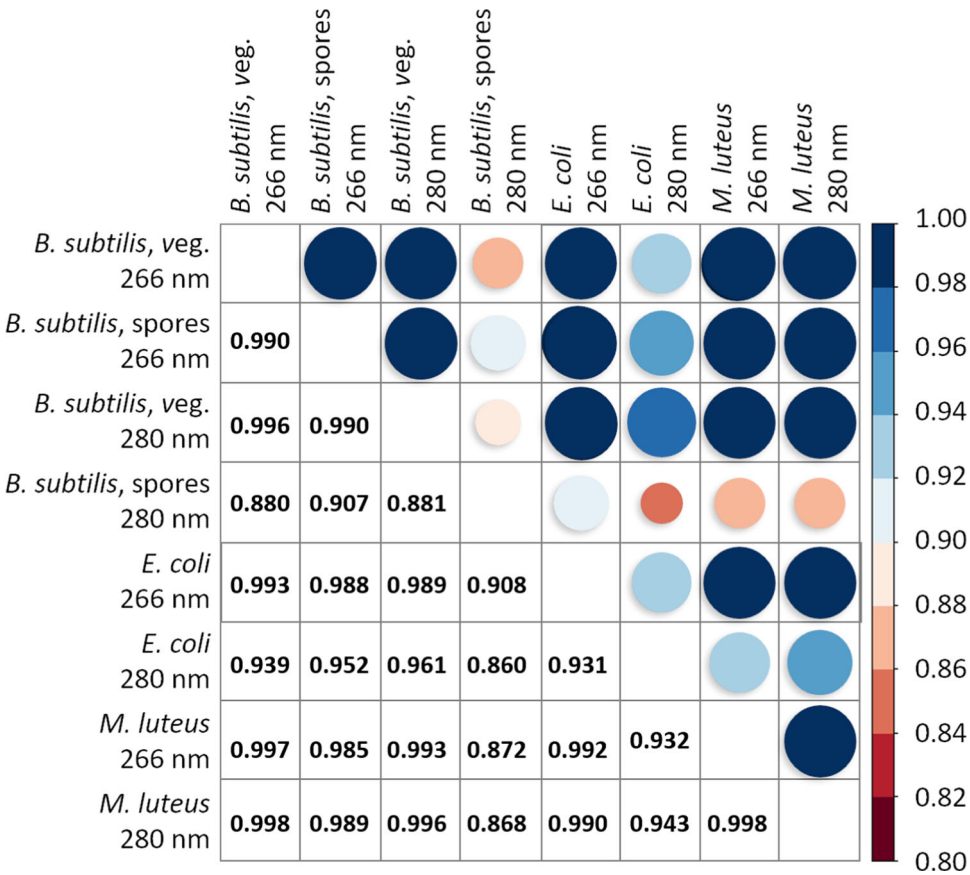

Fig. 13 Correlation matrix for the investigated spectra of bacteria fluorescence cross-sections

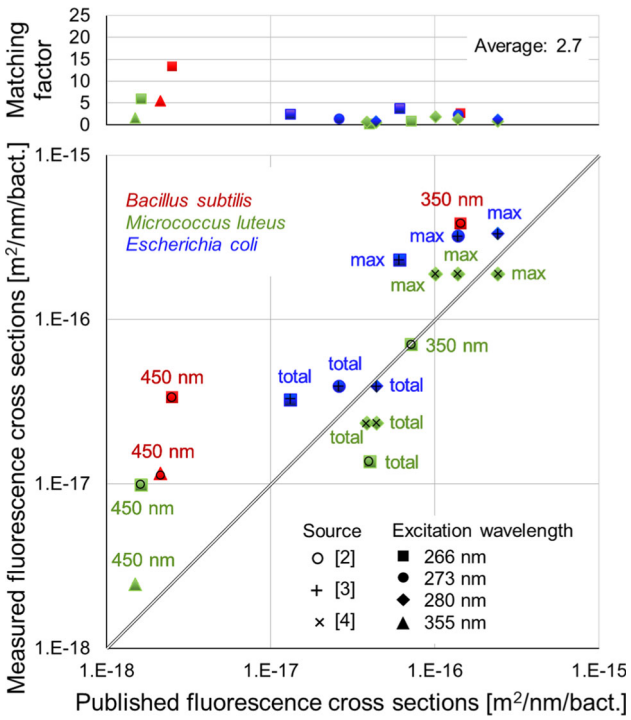

Fig. 14 Comparison of derived cross-section data with referenced values from the literature. Values integrated over the spectral range are referred to as "total." Maximum spectral values positioned at any wavelength are referred to as "max"

excitation-emission maps. As long as optical artifacts cannot be completely eliminated from the readings, the gathered cross-section datasets are affected by measuring errors difficult to recognize. Since such artifacts depend on the particular measuring system and are often hard to detect and to extract from measuring results, detailed analyses and comparisons of cross-section data have to be

performed within the same system setup to assess the results thoroughly. The spectral and total values of single bacteria fluorescence cross-sections are both essential for determining the strength of bacteria fluorescence response. To a vast extent, the fluorescence cross-sections presented in this paper are in satisfying agreement with data from the literature. Matching factors below 3.8 are achieved at an average of 1.6. Reasons for wider deviations at specific wavelengths of the spectra with matching factors between 5.5 and 13 can be attributed to the application of different calibration methods and to spectral polarization effects in the particular measuring system. The cross-section spectra of the vegetative cells show very strong correlations with correlation factors above 0.9. A slightly lower correlation is found between specific cross-section spectra of vegetative cells and spores. But nonetheless, correlation coefficients around 0.9 and above challenge any effort toward a discrimination of bacteria by fluorescence techniques.

Acknowledgements The authors thank their DLR coworkers Kirsten Klaffki for his intensive work on microscopical analyses, his support in the test campaigns, and his quality management, Björn Prietzel for the preparation of the chemical samples and the elaborated quality assurance system, and Lara-Cathrin Walprecht for the thorough preparation of the bacteria samples. Furthermore, we thank Günter Straube from the WIS for his contribution to the visualization of bacterial filter occupancies, and his continued support in all issues concerning scanning electron microscopy.

Author contributions Frank Duschek and Frank Wilsenack worked in supervison. Thomas Hall contributed to Mie modeling. Karin Grünewald and Thomas Hall helped in design and conduction of experiments. Karin Grünewald, Thomas Hall, Lea Fellner, Arne Walter, Marian Kraus, Frank Duschek, and Frank Wilsenack helped in data analysis and interpretation. Karin Grünewald, Thomas Hall, Lea Fellner, Arne Walter, Marian Kraus, Frank Duschek, and Frank Wilsenack contributed to manuscript writing and reviewing.

Funding Open Access funding enabled and organized by Projekt DEAL. No funding was received for conducting this study.

Materials availability Not applicable.

Data Availability Statement This manuscript has associated data in a data repository. [Authors' comment: The data that support the findings of this study are available from the corresponding author, Karin Grünewald, upon reasonable request].

Declarations

Conflict of interest The authors have no conflict of interest to declare that are relevant to the content of this article.

Ethics approval and consent to participate Not applicable.

Consent for publication Not applicable.

References

1. M. Seaver, D.C. Roselle, J.F. Pinto, J.D. Eversole, Absolute emission spectra from bacillus subtilis and escherichia coli vegetative cells in solution. Appl. Opt. **37**(22), 5344 (1998). https://doi.org/10.1364/ao.37.005344
2. V. Sivaprakasam, A.L. Huston, C. Scotto, Eversole, Multiple uv wavelength excitation and fluorescence of bioaerosols. Opt. Express **12**(19), 4457 (2004). https://doi.org/10.1364/opex.12.004457
3. Y.-L. Pan, S.C. Hill, J.L. Santarpia, K. Brinkley, T. Sickler, M. Coleman, C. Williamson, K. Gurton, M. Felton, R.G. Pinnick, N. Baker, J. Eshbaugh, J. Hahn, E. Smith, B. Alvarez, A. Prugh, W. Gardner, Spectrally-resolved fluorescence cross sections of aerosolized biological live agents and simulants using five excitation wavelengths in a bsl-3 laboratory. Opt. Express **22**(7), 8165 (2014). https://doi.org/10.1364/oe.22.008165
4. Y.-L. Pan, Detection and characterization of biological and other organic-carbon aerosol particles in atmosphere using fluorescence. J. Quant. Spectrosc. Radiat. Transf. **150**, 12–35 (2015). https://doi.org/10.1016/j.jqsrt.2014.06.007
5. G.W. Faris, R.A. Copeland, K. Mortelmans, B.V. Bronk, Spectrally resolved absolute fluorescence cross sections for bacillus spores. Appl. Opt. **36**(4), 958 (1997). https://doi.org/10.1364/ao.36.000958
6. A. Manninen, M. Putkiranta, J. Saarela, A. Rostedt, T. Sorvajärvi, J. Toivonen, M. Marjamäki, J. Keskinen, R. Hernberg, Fluorescence cross sections of bioaerosols and suspended biological agents. Appl. Opt. **48**(22), 4320 (2009). https://doi.org/10.1364/ao.48.004320
7. R. Weichert, W. Klemm, K. Legenhausen, C. Pawellek, Determination of fluorescence cross-sections of biological aerosols. Part. Part. Syst. Charact. Meas. Descr. Part Prop Behav. Powders Other Dispers Syst. **19**(3), 216 (2002)
8. U. Brackmann, Lambdachrome Laser Dyes, 3rd edn. https://api.semanticscholar.org/CorpusID:136745736 (1985)
9. W.J. Wiscombe, Improved Mie scattering algorithms. Appl. Opt. **19**(9), 1505 (1980). https://doi.org/10.1364/ao.19.001505
10. W. Wiscombe, Mie scattering calculations: advances in technique and fast, vector-speed computer codes. Technical report, University Corporation for Atmospheric Research. (1979). https://doi.org/10.5065/D6ZP4414
11. C.F. Bohren, D.R. Huffman, *Absorption and scattering of light by small particles* (Wiley, 2008), pp.82–129
12. J. Heyder, J. Gebhart, Optimization of response functions of light scattering instruments for size evaluation of aerosol particles. Appl. Opt. **18**(5), 705 (1979). https://doi.org/10.1364/ao.18.000705
13. A. Hüttner, Berechnung der Streulichtsignale von Kugeln für verschiedene Geometrien der optischen Messanordnung. mathesis, Clausthal University of Technology (1991)

14. T. Inagaki, E.T. Arakawa, R.N. Hamm, M.W. Williams, Optical properties of polystyrene from the near-infrared to the x-ray region and convergence of optical sum rules. Phys. Rev. B **15**(6), 3243–3253 (1977). https://doi.org/10.1103/physrevb.15.3243
15. E.R. Peck, K. Reeder, Dispersion of air. JOSA **62**(8), 958 (1972). https://doi.org/10.1364/josa.62.000958
16. G.M. Hale, M.R. Querry, Optical constants of water in the 200-nm to 200-μm wavelength region. Appl. Opt. **12**(3), 555 (1973). https://doi.org/10.1364/ao.12.000555
17. HeraeusConamic: fused quartz and fused silica for optical applications. https://www.heraeus-conamic.com (2024)
18. G.W. Faris, R.A. Copeland, Wavelength dependence of the Raman cross section for liquid water. Appl. Opt. **36**(12), 2686 (1997). https://doi.org/10.1364/ao.36.002686
19. S.R. Pattenaude, L.M. Streacker, D. Ben-Amotz, Temperature and polarization dependent Raman spectra of liquid h_2o and d_2o. J. Raman Spectrosc. **49**(11), 1860–1866 (2018). https://doi.org/10.1002/jrs.5465
20. E. Trinquet, G. Mathis, Fluorescence technologies for the investigation of chemical libraries. Mol. BioSyst. **2**, 380–387 (2006). https://doi.org/10.1039/B607152J
21. J.W. Oblanas, D. Ross, V.F. Simmon, F.L. Ludwig, M. Anbar, Optical techniques for the remote detection of biological aerosols. Technical report, Edgewood Arsenal Contract Report ED-CR-74021 (1974)
22. Hamamatsu: Photomultiplier Tubes - Basics and Applications (2007)
23. T. Saito, Spectral Properties of Semiconductor Photodiodes. InTech. https://doi.org/10.5772/15300 (2011)
24. K. Hoffmann, N. Nirmalananthan-Budau, U. Resch-Genger, Fluorescence calibration standards made from broadband emitters encapsulated in polymer beads for fluorescence microscopy and flow cytometry. Anal. Bioanal. Chem. **412**(24), 6499–6507 (2020). https://doi.org/10.1007/s00216-020-02664-y
25. F. Gebert, M. Kraus, L. Fellner, A. Walter, C. Pargmann, K. Gruenewald, F. Duschek, Novel standoff detection system for the classification of chemical and biological hazardous substances combining temporal and spectral laser-induced fluorescence techniques. Eur. Phys. J. Plus (2018). https://doi.org/10.1140/epjp/i2018-12147-2
26. J.A. Huffman, A.E. Perring, N.J. Savage, B. Clot, B. Crouzy, F. Tummon, O. Shoshanim, B. Damit, J. Schneider, V. Sivaprakasam, M.A. Zawadowicz, I. Crawford, M. Gallagher, D. Topping, D.C. Doughty, S.C. Hill, Y. Pan, Real-time sensing of bioaerosols: review and current perspectives. Aerosol Sci. Technol. **54**(5), 465–495 (2020). https://doi.org/10.1080/02786826.2019.1664724
27. J.R. Stephens, Measurements of the ultraviolet fluorescence cross sections and spectra of bacillus anthracis simulants. Los alamos national lab report 19990628 028, Los Alamos National Laboratory (1999)
28. J. Kunnil, S. Sarasanandarajah, E. Chacko, L. Reinisch, Fluorescence quantum efficiency of dry bacillus globigii spores. Opt. Express **13**(22), 8969 (2005). https://doi.org/10.1364/opex.13.008969